ISSN Online: 2756-3898, ISSN Print: 2714-500X https://doi.org/10.47514/phyaccess.2025.5.2.005

High Order Harmonic Generation using Inhomogeneous Two Colour Field, Polarization Gating and Static Electric Field

Onsure D Nyang'au[1], Kebwaro J Monari[1], Rurimo G Kihara[2] and Njoroge S Maina[1]

[1] Department of Physical and Biological Sciences, Karatina University, P.O. Box 1957-10101, Karatina, Kenya
[2] National Institute of Optics and Laser, Multimedia University of Kenya, P.O. Box 1957-10101, Nairobi, Kenya

Corresponding E-mail: snjoroge@karu.ac.ke

Received 24-07-2025
Accepted for publication 11-09-2025
Published 15-09-2025

Abstract

In this study, high-order harmonic generation was investigated under the combined influence of three enhancement schemes: a plasmonic-enhanced two colour field, modulated polarization gating, and a static electric field. Numerical simulations based on the one-dimensional time-dependent Schrödinger equation (1D-TDSE) were carried out to analyze the influence of field inhomogeneity, polarization modulation, and electron trajectory control on harmonic spectra. The analysis demonstrates that an increase in the inhomogeneity parameter, together with precise tuning of the polarization angle, produces extended harmonic cut-offs and more intense bursts near peak field cycles. The introduction of a static electric field further improved the harmonic conversion efficiency, while the combined application of all three mechanisms yields harmonic spectra characterized by two distinct plateaus, broadened spectral bandwidths, and significantly higher emission yields. A high harmonic cut-off reaching the 600^{th} order is observed in the first plateau, while the second plateau extends beyond the 1550^{th} order. Time-frequency spectrograms reveal well-defined harmonic bursts and high-energy electron recollisions contributing to this extension. These findings confirm that the synergy of polarization gating, plasmonic field enhancement and static field confinement offers a robust pathway for generating bright and broadband extreme ultraviolet (XUV) continua, which are essential for advancing attosecond pulse generation and ultrafast spectroscopy.

Keywords: High order harmonic generation; Conversion efficiency; cut-off point; Harmonic Spectrum.

I. INTRODUCTION

The quest to understand and manipulate ultrafast dynamical processes in matter on ever-shorter timescales has driven significant progress in the field of ultrafast physics. Among the most transformative developments is high-order harmonic generation (HHG), a nonlinear process in which a strongly focused laser field interacts with matter [1–4], producing coherent radiation at frequencies that are integer multiples of the fundamental laser frequency [1, 2, 5]. Over the past decades, HHG has been studied extensively, both experimentally [6–9] and theoretically [10–12], owing to its ability to generate extreme ultraviolet (XUV) light [5, 13], soft X-rays [14, 15], and attosecond pulses [16–20]. Attosecond pulses, which last less than one attosecond (10^{-18} s), represent one of the most significant advances in laser science, enabling

 ©DOP_KASU Publishing

unprecedented insights into the fundamental principles of light–matter interactions [18]. In particular, the generation of isolated attosecond pulses through HHG [19, 20] has attracted wide interest because of its potential applications in attosecond spectroscopy [19–21] and in probing ultrafast electronic and structural dynamics in atoms [1, 2] and molecules [22–24]. Despite these advances, HHG remains severely limited by its intrinsically low conversion efficiency.

One approach to attosecond pulse generation is to employ intense multi-cycle laser fields and subsequently select multiple harmonics within the plateau region [16]. To address the limitations in efficiency, several enhancement techniques have been proposed, including the use of plasmonically enhanced laser fields [25–28] and static electric fields [25, 29, 30]. In plasmonic enhancement schemes, the motion of electrons can be steered using two or more laser pulses of different wavelengths combined into a complex driving field [31]. This approach eliminates the need for additional amplification cavities [16, 32] while simultaneously enhancing local field intensities by more than 20 dB [33]. As a result, HHG can be achieved even below the typical threshold intensity of ~10^{13} W/cm². The technique is not only relatively simple and cost-effective [28, 34], but it has also found applications in fields ranging from the study of ultrafast chemical dynamics [1, 2, 35] to efficient high-order harmonic production [34].

The application of a static electric field has also been shown to significantly influence HHG efficiency. When applied along the laser polarization axis, the static field suppresses the transverse spreading of the electron wave packet [25, 29, 30, and 36]. For instance, a study of HHG from a helium ion model driven by a two colour field composed of a fundamental pulse and its second harmonic, demonstrated the generation of a super continuum spectrum, albeit with relatively low spectral intensity [25]. Upon introducing a static electric field, however, the ionization yield of electrons contributing to harmonic emission was dramatically increased. This modification enhanced the quantum pathways of HHG, resulting in an extended and intensified super continuum with a bandwidth of approximately 170.5 eV [25].

Although HHG in rare gases has been widely proposed as a compact tabletop source of coherent XUV radiation [1, 37, 38], gaseous media inherently suffer from low conversion efficiency due to their irregular structure and relatively low density [39]. This shortcoming is a critical obstacle in applications that demand high photon flux. According to the semi classical three-step model of HHG, first established over 30 years ago [39], the strong laser field distorts the atomic potential barrier, allowing tunnel ionization. The liberated electron then oscillates along the laser polarization axis and, upon recombination with the parent ion, emits its excess energy as XUV radiation. The intensity of the resulting XUV signal depends not only on this microscopic process but also on the macroscopic phase matching between the driving laser field and the generated harmonics [15].

This work investigates the enhancement of HHG in neon gas through the simultaneous implementation of three complementary schemes: plasmonic-enhanced two colour fields, polarization gating, and the application of a static electric field. The study further demonstrates that both the intensity and spectral characteristics of high-order harmonics can be effectively manipulated by tuning the laser polarization orientation, adjusting the inhomogeneity parameter, and incorporating a static electric field into the interaction.

II. THEORETICAL MODEL

This study employed numerical simulations to generate harmonic spectra by solving the one-dimensional time-dependent Schrödinger equation (1D-TDSE). The 1D-TDSE effectively captures the essential physics of strong-field interactions between the driving laser field and the atomic electron, while reducing computational complexity [40]. The equation is given as follows.

$$\left[i\frac{\partial\Psi(x,t)}{\partial t} = H(x,t)\Psi(x,t)\right] \quad (1)$$

$$= \left[-\frac{1}{2}\frac{\partial^2}{\partial x^2} + V_a(x) + V_i(x,t)\right]\Psi(x,t) \quad (2)$$

Where $V_a(x) = -\frac{1}{\sqrt{x^2+\alpha}}$ is a soft-core potential and $V_l(x,t) = -E_x(x,t)x$ is the potential due to electron interaction. The soft core parameter α was chosen to be 0.1195 to match the ground ionization potential of neon atom which is 0.7925 a.u (21.6 eV).

The x component of the inhomogeneous field is given by:

$$E_x(x,t) = E_x(t)\left(1+\varepsilon_x(x)\right) \quad (3)$$

Here the parameter ε_x defined the strength inhomogeneity of the laser field along the x direction [41].

The electric field of the x component of the two colour field is given as:

$$E(t) = (\beta E_o + E_o[f_1(t)\cos(\omega_o t + \varphi(t)) + f_2(t)\cos(2\omega_o t + \varphi(t))]e_x \quad (4)$$

Here β is the ratio of the static electric field and the laser field, E_o is the amplitude of laser field, while f_1 (t) and f_2 (t) represent the pulse envelopes.

The split-operator method [42] was used to solve (1). To avoid incorrect reflections from the boundaries, the electron wave-function was multiplied by a mask function at each time step [43]. The neon atom was in the initial (ground) state before the laser is turned on. The ground state is obtained by imaginary time propagation with the soft-core potential. Once the electron wave function ψ (x, t) is obtained, the time-dependent dipole acceleration along x direction was calculated by the Ehrenfest theorem [44].

$$a_x(t) = -\langle\varphi(x,t)|[H(x,t),[H(x,t),x]]|\varphi(x,t)\rangle \quad (5)$$

The HHG spectrum was obtained by Fourier transforming time-dependent dipole acceleration given as;

$$\left|S_{qx}(\omega)\right|^2 = \left|\frac{1}{T}\int_0^T a_x(t)e^{-iq\omega t}dt\right|^2 \quad (6)$$

Time-frequency analysis by means of wavelet transform (WT) is used to analyze the numerically generated HHG spectrum [43]. The equation is given as;

$$A(t,\omega) = \int d_a(t)\sqrt{\omega}W[\omega(t'-t)]dt' \qquad (7)$$

Where d_a is the time dependent dipole acceleration and $W[\omega(t'-t)]$ is the mother wavelet. A natural choice of the mother wavelet is given by the mother Morlet wavelet;

$$\omega W[\omega(t'-t)] = \frac{1}{\sqrt{\pi^{\frac{1}{2}}\sigma}}\exp(i\omega(t'-t)\exp\left(\frac{-\omega^2(t'-t)^2}{2\sigma^2}\right) \qquad (8)$$

Here, σ is the Gaussian width which was set to be 2π.

The study finally obtained the isolated attosecond pulse by superposing several harmonic orders as;

$$\left[I_x(t) = \left|\sum_q S_{qx}\, e^{iq\omega t}dt\right|^2\right] \qquad (9)$$

Where q is the harmonic order (the harmonic orders derived by performing an inverse Fourier transformation of the XUV super continuum in different spectral regions).

III. RESULTS AND DISCUSSIONS

Fig. 1(a) presents the components of the generated harmonic spectrum in a homogeneous two colour field for varying polarization angles (θ): 0.2π (blue line), 0.4π (red line), and 0.6π (green line). Fig. 1(b–d) display the corresponding frequency-time distributions for the harmonic spectra shown in Fig. 1(a). The other optimized parameters are as follows: Fundamental wavelength, E_0 = 700 nm, Control wavelength, E_1 = 2000 nm, Fundamental field intensity, $I_0 = 8.5 \times 10^{14}$ W/cm² and Control field intensity, $I_1 = 7.65 \times 10^{14}$ W/cm².

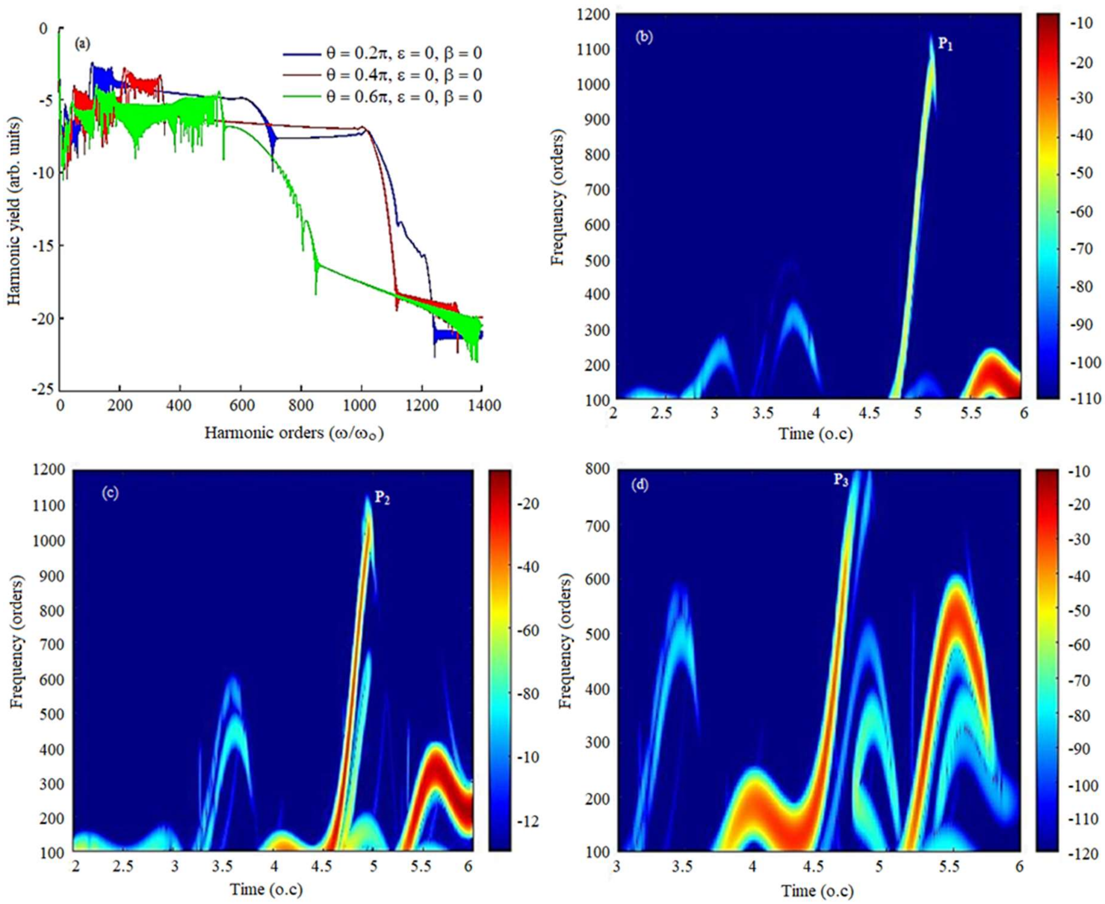

Fig. 1. (a) The components of the generated harmonic spectrum in the homogeneous two colour field for different polarization angles and (b)-(d) the corresponding time frequency distributions for the generated harmonic spectrum.

In this simulation, only the polarization angle (θ) is varied, while both the inhomogeneity parameter (ε) and the static electric field (β) are kept constant at zero. Fig. 1(a) shows that when the polarization angle, θ = 0.2π (blue line), the spectrum exhibits the broadest plateau and the highest cut-off, extending beyond 1000th harmonic orders, indicating favorable conditions for electron excursion and recombination. As the polarization angle increases to 0.4π, the cut-off decreases slightly, though the plateau remains pronounced, suggesting partial suppression of long trajectories. At $\theta = 0.6\pi$, the cut-off drops further to about 850th harmonic orders, and the spectrum becomes more irregular, reflecting destructive interference between electron trajectories. The spectrum observations are confirmed by the frequency-time distributions in Fig. 1(b), (c), and (d), which correspond to the spectrum for the polarization angles of 0.2π, 0.4π, and 0.6π, respectively, as observed in Fig. 1(a). Fig. 1(b) reveals a sharp, intense burst of high-order harmonics around 4.8 optical cycles labeled as peak P_1. This emission rapidly extends beyond the 1000th harmonic order, indicating interaction at peak laser intensity. The narrow, chirped structure suggests efficient electron acceleration and recombination, characteristic of cut-off harmonics and potential attosecond pulse generation. The steep rise in frequency reflects the strong temporal gradient of the driving field. After 5.5 o.c, the emission weakens and shifts to lower orders due to decreasing field strength and ionization effects. This localized peak demonstrates the nonlinear dynamics governing high-efficiency HHG near the pulse maximum. Fig. 1(c) shows a spectrogram with harmonic peak P_2, which is slightly less energetic compared to peak P_1, suggesting electron path interferences. The spectrogram in Fig. 1(d) reveals a less energetic and lower-reaching high-order harmonic burst, peak P_3, compared to the previous harmonic peaks P_1 and P_2. The peak emission occurs around 4.6 optical cycles, reaching up to about 850th harmonic order, with broader time-frequency spread and reduced intensity. The plateau is more pronounced at lower orders, between 100–300 harmonic orders, and post-peak emission (after 5 o.c) is stronger. Compared to the spectrogram in Fig. 1(c), the cut-off extends to lower orders and shows less localization, indicating reduced driving field intensity or less efficient phase matching. From the observations made, the polarization angle, θ = 0.2π is considered as optimal for the next simulations.

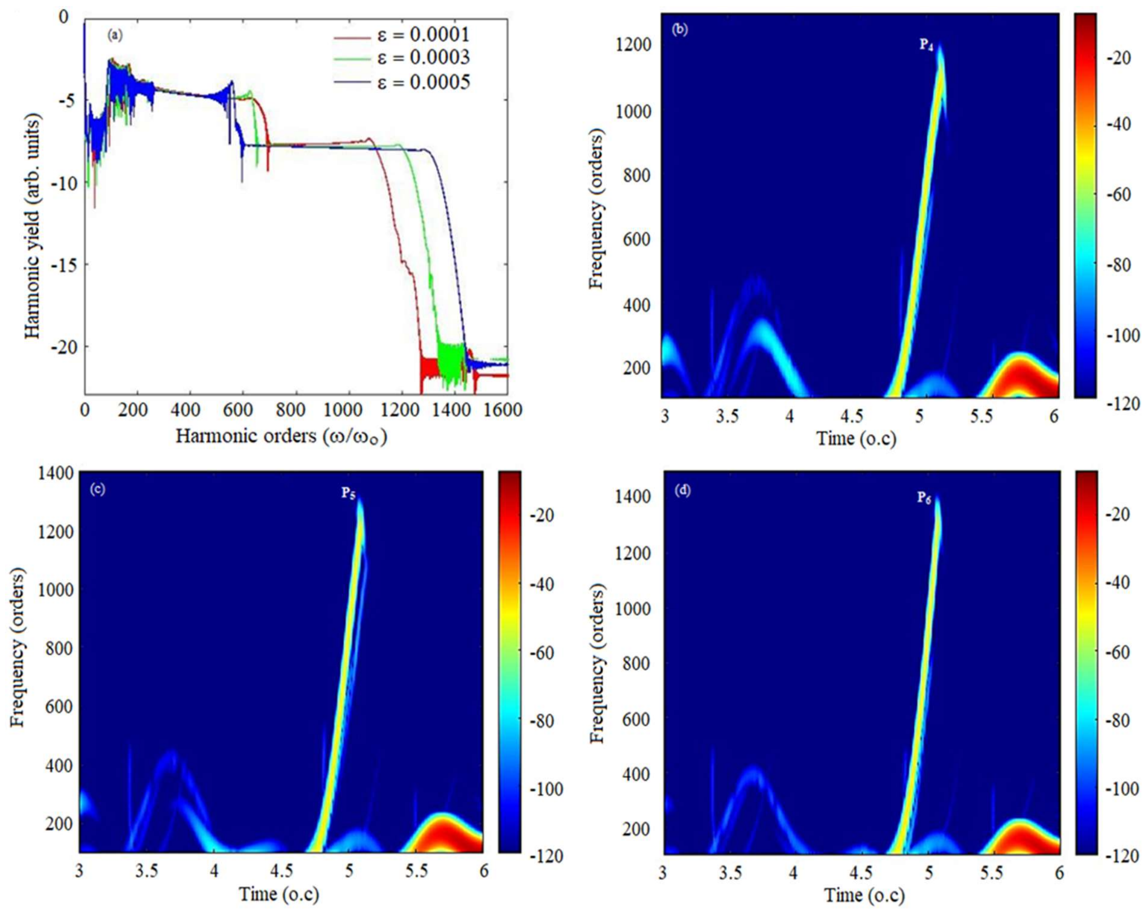

Fig. 2. (a) The component of the generated harmonic spectrum in the inhomogeneous two colour field for different inhomogeneity parameters and (b), (c) and (d) the corresponding time frequency distributions for the generated harmonic spectrum.

Fig. 2(a) displays the components of the generated harmonic spectrum for a two colour field with plasmonic enhancement, achieved by varying inhomogeneity parameter **ε**. The corresponding frequency-time distributions are shown in Fig. 2(b–d). Here, only the inhomogeneity parameter ε is varied, while, all other parameters are maintained as in Fig. 1(a): E_0 = 700 nm, E_1 = 2000 nm, $I_0 = 8.5 \times 10^{14}$ W/cm², $I_1 = 7.65 \times 10^{14}$ W/cm², θ = 0.2π (optimized) and β = 0 (static electric field remains zero).

The harmonic spectrum and corresponding time-frequency spectrograms demonstrate the significant impact of the inhomogeneity parameter ϵ on high-order harmonic generation. The spectrum presents three curves for $\epsilon = 0.0001, 0.0003,$ and 0.0005, where increasing ϵ leads to a significant extension of the harmonic cut-off from below the 1000th order (red curve) to beyond the 1400th order (blue curve). This trend indicates enhanced electron acceleration and energy gain under stronger field conditions, consistent with the semi-classical three-step model of HHG. The spectrograms offer time-resolved insight into these spectral differences. For $\epsilon = 0.0001$, the harmonic burst, peak P_4 is weaker and terminates near the 1000th order. The emission is relatively broad in time and shows limited vertical extension, implying lower efficiency and a narrower cut-off region. At $\epsilon = 0.0003$, the second spectrogram displays a more pronounced and temporally confined burst, peak P_5 near 5.0 optical cycles, reaching above the 1200th harmonic order. This suggests stronger interaction and better phase matching. For $\epsilon = 0.0005$, the final spectrogram exhibits the most intense and vertically extended harmonic burst, peak P_6, reaching nearly the 1400th order. The structure is sharp and narrow in time, consistent with a highly localized emission near the peak laser field. This behaviour matches the broad, flat plateau and extended cut-off in the blue spectral curve, confirming efficient HHG and possibly isolated attosecond pulse generation.

Collectively, these results demonstrate that increasing the inhomogeneity parameter enhances both the efficiency and temporal localization of high-order harmonic generation. This enables higher-order emission and provides improved control over ultrafast light sources.

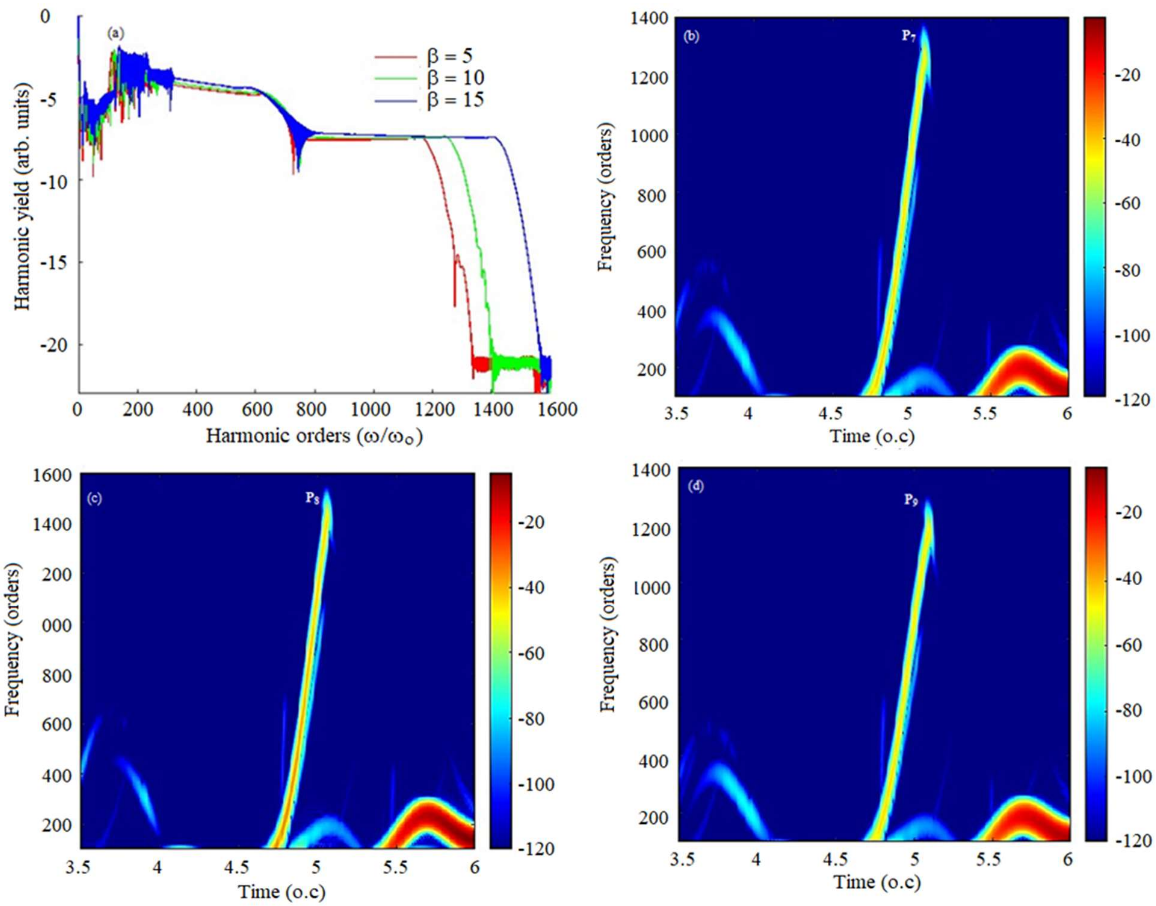

Fig. 3. (a) The component of the generated harmonic spectrum in the inhomogeneous two colour field with static electric field and (b-d) the corresponding time frequency distributions for the generated harmonic spectrum.

The results in Fig. 3(a) show the component of the generated harmonic spectrum when using inhomogeneous two colour fields for different values of the static electric field while Fig. 3 (b)-(d) show the corresponding time frequency distributions for the harmonic spectrum. Here, all other parameters are maintained as those used in Fig. 2 but inclusive of the optimized inhomogeneity parameter, $\varepsilon = 0.0005$. The harmonic spectrum illustrates the effect of a static electric field (quantified by β) on high-order harmonic generation. Three values are considered: β=5(red line), β=10 (green line), and β=15 (blue line). As the strength of the static field increases, there is a marked enhancement in both the harmonic yield and the cut-off energy. For β=5, the harmonic plateau extends up to approximately the 1250th harmonic order, beyond which a rapid decline in yield occurs. Increasing the static field to β=10 shifts the cut-off to about the 1400th order, indicating greater electron acceleration and recombination energies. At $\beta = 15$, the cut-off reaches nearly the 1600th harmonic order, with a notably extended and flatter plateau, reflecting more efficient and prolonged HHG.

The static electric field plays a crucial role by modifying the electron trajectories after ionization. A stronger static field (β) biases the continuum dynamics, allowing electrons to gain more energy before recombining with the parent ion. This leads to both higher-energy photon emission and improved phase matching conditions. The trend is consistent with time-frequency analyses, where higher static fields produce sharper, more energetic bursts of harmonic emission.

The three spectrograms presented in Fig. 3(b)-(d) correspond directly to the harmonic spectra shown earlier in Fig. 3(a), where the static electric field strength is varied as $\beta = 5, 10$, and 15. Each spectrogram reveals the temporal dynamics of high-order harmonic generation, providing insight into the timing and frequency distribution of harmonic bursts responsible for the observed spectra. In all three cases, a prominent harmonic burst appears around 5 optical cycles (o.c.), indicating the primary ionization-recollision event responsible for the highest energy harmonics. As β increases, both the intensity and frequency range of the harmonic burst extend significantly. For $\beta = 5$ as observed in Fig. 3(b), the burst, peak P_7 reaches a maximum frequency of about the 1250th harmonic order. When β is increased to 10 as seen in Fig. 3(c), the harmonic cut-off extends to approximately the 1450th order with harmonic peak P_8. At the highest value, $\beta = 15$ (Fig. 3 (d)), the burst, peak P_9, reaches the 1600th order, consistent with the cut-off observed in the corresponding spectrum. This trend reflects the role of the static electric field in modifying the electron trajectories during HHG. A stronger static field (higher β) increases the potential energy of the ionized electron and enhances its acceleration, allowing it to gain more kinetic energy before recombination. Consequently, this results in a higher harmonic cut-off and a broader plateau in the spectrum. Furthermore, the bursts are temporally localized, mainly occurring around 5 o.c., regardless of β. However, the intensity and duration of the bursts increase with β, as evidenced by the stronger and more extended high-frequency structures in the spectrograms. This implies that the static field not only increases the maximum photon energy but also improves the efficiency of HHG by enhancing phase-matching and electron return conditions.

Generally, the spectrograms illustrate how increasing the static field strength β enhances both the harmonic cut-off and the efficiency of HHG. The harmonic bursts become more intense and extend to higher frequencies, consistent with the observed spectral cut-offs observed in the corresponding spectra.

IV. CONCLUSION

In conclusion, our analysis demonstrates the significant influence of both the polarization angle (θ), inhomogeneity parameter (ε) and the static electric field strength (β) on the high-order harmonic generation process. The harmonic spectra indicate that lower polarization angles and increased inhomogeneity enhance the harmonic cut-off, shifting the maximum yield toward higher harmonic orders. This spectral broadening correlates with the time-frequency spectrograms, which show intense and temporally localized harmonic bursts occurring around 5 optical cycles (o.c.), where the highest-energy recollision events dominate. The addition of a static electric field (β) further extends the harmonic cut-off, as evidenced by both the spectra and spectrograms. The cut-off increases from the 1250th to approximately the 1600th order, at $\beta = 5$ and $\beta = 15$, respectively, reflecting enhanced electron kinetic energy due to the static field. Spectrograms confirm that stronger static fields not only increase cut-off energy but also intensify harmonic bursts and improve HHG efficiency. Overall, the combined effects of polarization angle, inhomogeneity and static field strength offers a powerful means of controlling harmonic generation, enabling the production of broader and more intense extreme ultraviolet spectra, which are vital for attosecond pulse generation and ultrafast spectroscopy.

ACKNOWLEDGMENT

The authors acknowledge Karatina University for providing the facilities and resources required to conduct this research.

References

[1] R. A. Ganeev, "High-order harmonic generation in laser-induced low-density plasma: past and recent achievements," *Applied Physics B*, vol. 129, no. 1, Dec. 2022, doi: https://doi.org/10.1007/s00340-022-07960-2.

[2] J. Gao *et al.*, "High-order harmonic generation in an x-ray range from laser-induced multivalent ions of noble gas," *Optica*, vol. 9, no. 9, pp. 1003–1003, Aug. 2022, doi: https://doi.org/10.1364/optica.456481.

[3] O. Neufeld, Zahra Nourbakhsh, N. Tancogne-Dejean, and A. Rubio, "Ab Initio Cluster Approach for High Harmonic Generation in Liquids," *Journal of Chemical Theory and Computation*, vol. 18, no. 7, pp. 4117–4126, Jun. 2022, doi: https://doi.org/10.1021/acs.jctc.2c00235.

[4] J. Park, A. Subramani, S. Kim, and M. F. Ciappina, "Recent trends in high-order harmonic generation in solids," *Advances in Physics: X*, vol. 7, no. 1, Dec. 2021, doi: https://doi.org/10.1080/23746149.2021.2003244.

[5] G. S. Boltaev, M. Iqbal, N. A. Abbasi, V. V. Kim, R. A. Ganeev, and A. S. Alnaser, "Enhanced XUV harmonics generation from diatomic gases using two orthogonally polarized laser fields," *Scientific Reports*, vol. 11, no. 1, Mar. 2021, doi: https://doi.org/10.1038/s41598-021-85114-8.

[6] S. Ren *et al.*, "Plasmon-Enhanced Circular Polarization High-Harmonic Generation from Silicon," *Advanced Optical Materials*, vol. 12, no. 31, Aug. 2024, doi: https://doi.org/10.1002/adom.202401478.

[7] M. Iqbal, G. S. Boltaev, N. Abbasi, R. A. Ganeev, and A. S. Alnaser, "Spatial and spectral variations of high-order harmonics generated in noble gases," *Journal of Physics B: Atomic, Molecular and Optical Physics*, vol. 55, no. 10, p. 105601, May 2022, doi: https://10.0.4.64/1361-6455/ac69c1.

[8] P.-A. . Chevreuil *et al.*, "Water-window high harmonic generation with 0.8-µm and 2.2-µm OPCPAs at 100 kHz," *Optics Express*, vol. 29, no. 21, p. 32996, Sep. 2021, doi: https://doi.org/10.1364/OE.440273.

[9] M. Davino *et al.*, "Higher-order harmonic generation and strong field ionization with Bessel–Gauss beams in a thin jet geometry," *Journal of the Optical Society of America B*, vol. 38, no. 7, pp. 2194–2194, Jun. 2021, doi: https://10.0.5.84/josab.420073.

[10] L. Li, P. Lan, X. Zhu, and P. Lu, "Huygens-Fresnel Picture for High Harmonic Generation in Solids," *Physical review letters (Print)*, vol. 127, no. 22, Nov. 2021, doi: https://doi.org/10.1103/PhysRevLett.127.223201

[11] L. Yue, L. Yue, M. B. Gaarde, and M. B. Gaarde, "Introduction to theory of high-harmonic generation in solids: tutorial," *JOSA B*, vol. 39, no. 2, pp. 535–555, Feb. 2022, doi: https://doi.org/10.1364/JOSAB.448602.

[12] L. Yue and M. B. Gaarde, "Expanded view of electron-hole recollisions in solid-state high-order harmonic generation: Full-Brillouin-zone tunneling and imperfect recollisions," *Physical review*, vol. 103, no. 6, Jun. 2021, doi: https://doi.org/10.1103/physreva.103.063105.

[13] F. Krausz and M. Ivanov, "Attosecond physics," *Reviews of Modern Physics*, vol. 81, no. 1, pp. 163–234, Feb. 2009, doi: https://doi.org/10.1103/revmodphys.81.163.

[14] Sylvianne D. C. Roscam Abbing, F. Campi, A. Zeltsi, P. Smorenburg, and P. M. Kraus, "Divergence and efficiency optimization in polarization-controlled two colour high-harmonic generation," *Scientific Reports*, vol. 11, no. 1, Dec. 2021, doi: https://doi.org/10.1038/s41598-021-03657-2.

[15] T. Popmintchev *et al.*, "Bright Coherent Ultrahigh Harmonics in the keV X-ray Regime from Mid-Infrared Femtosecond Lasers," *Science*, vol. 336, no. 6086, pp. 1287–1291, Jun. 2012, doi: https://doi.org/10.1126/science.1218497.

[16] S. Njoroge and D. Kinyua, "High-order harmonic generation in a doped semiconductor by inhomogeneous laser field," *Applied physics. B, Lasers and optics*, vol. 130, no. 6, Jun. 2024, doi: https://doi.org/10.1007/s00340-024-08251-8.

[17] R. Weissenbilder *et al.*, "How to optimize high-order harmonic generation in gases," *Nature Reviews Physics*, vol. 4, no. 11, pp. 713–722, Nov. 2022, doi: https://doi.org/10.1038/s42254-022-00522-7.

[18] E. Constant *et al.*, "High order harmonic generation-based attosecond light sources and applications to quantum phenomena," *APL Photonics*, vol. 10, no. 1, Jan. 2025, doi: https://doi.org/10.1063/5.0235171.

[19] X. Li, J. Han, L. Liu, X. Wang, G. Wang, and C. Jin, "Shaping extreme-ultraviolet attosecond pulses by tuning the minimum in high-order harmonic generation with two gas jets," *Physical review. A/Physical review, A*, vol. 109, no. 2, Feb. 2024, doi: https://doi.org/10.1103/physreva.109.023103.

[20] Yu. Ryabikin, Yu. Emelin, and V. Strelkov, "Attosecond electromagnetic pulses: generation, measurement, and application. Attosecond metrology and spectroscopy," *Physics-Uspekhi*, vol. 66, no. 04, pp. 360–380, Oct. 2021, doi: https://doi.org/10.3367/ufne.2021.10.039078.

[21] H. Liang, W.-D. Yu, L. Geng, and L.-Y. Peng, "Dynamical analysis of attosecond molecular modes," *Physical review. A/Physical review, A*, vol. 107, no. 1, Jan. 2023, doi: https://doi.org/10.1103/physreva.107.013101.

[22] X. Wang *et al.*, "Ultrashort isolated attosecond pulses generation with 750 nm free-CEP near-infrared pulses.," *Ultrafast Science*, Nov. 2024, doi: https://doi.org/10.34133/ultrafastscience.0080.

[23] S. Xiaohong *et al.*, "Control of the electron dynamics in solid-state high harmonic generation on ultrafast time scales by a polarization-skewed laser pulse," *Optics express*, vol. 31, no. 12, pp. 18862–18862, May 2023, doi: https://doi.org/10.1364/oe.491418.

[24] M. F. Ciappina *et al.*, "Attosecond physics at the nanoscale," *Reports on Progress in Physics*, vol. 80, no. 5, pp. 054401–054401, Mar. 2017, doi: https://doi.org/10.1088/1361-6633/aa574e.

[25] G.-T. Zhang, T.-T. Bai, and M.-G. Zhang, "Generation of an isolated sub-30 attosecond pulse in a two colour laser field and a static electric field," *Chinese Physics B*, vol. 21, no. 5, p. 054214, May 2012, doi: https://doi.org/10.1088/1674-1056/21/5/054214.

[26] K. Burnett and S. C. Rae, "Calculations of high-order-harmonic generation in the strongly ionizing regime," *Physical Review A*, vol. 48, no. 3, pp. 2490–2493, Sep. 1993, doi: https://doi.org/10.1103/physreva.48.2490.

[27] S. Kim, J. Jin, Y.-J. Kim, I.-Y. Park, Y. Kim, and S.-W. Kim, "High-harmonic generation by resonant plasmon field enhancement," *Nature*, vol. 453, no. 7196, pp. 757–760, Jun. 2008, doi: https://doi.org/10.1038/nature07012.

[28] L. Feng, M. Yuan, and T. Chu, "Attosecond x-ray source generation from two colour polarized gating plasmonic field enhancement," *Physics of Plasmas*,

vol. 20, no. 12, pp. 122307–122307, Dec. 2013, doi: https://doi.org/10.1063/1.4848757.

[29] A. M. Koushki and S. Sarikhani, “High-order harmonic generation from CH4 and CD4 molecules in the presence of a static electric field,” *Chemical Physics*, vol. 541, p. 111020, Oct. 2020, doi: https://doi.org/10.1016/j.chemphys.2020.111020.

[30] A. A. Silaev, A. A. Romanov, and N. V. Vvedenskii, “High Harmonic Generation from Oriented Asymmetric Molecules in the Presence of Static Electric Field,” *Journal of Physics Conference Series*, vol. 2249, no. 1, pp. 012004–012004, Apr. 2022, doi: https://doi.org/10.1088/1742-6596/2249/1/012004.

[31] X. Ren *et al.*, “Attosecond light sources in the water window,” *Journal of Optics*, vol. 20, no. 2, pp. 023001–023001, Dec. 2017, doi: https://doi.org/10.1088/2040-8986/aaa394.

[32] F. Salmeh and M. Mohebbi, “Generation of a single attosecond pulse by gaseous atoms in a conical plasmonic nanostructure using a radially polarized laser beam,” *Optics & Laser Technology*, vol. 170, p. 110319, Nov. 2023, doi: https://doi.org/10.1016/j.optlastec.2023.110319.

[33] H. Yuan, L. He, F. Wang, B. Wang, W. Liu, and Z. Hong, “Generation of isolated attosecond pulses in a multi-cycle inhomogeneous two colour field without CEP stabilization,” *Optical and Quantum Electronics*, vol. 49, no. 6, May 2017, doi: https://doi.org/10.1007/s11082-017-1048-x.

[34] H. Vincenti, S. Monchocé, S. Kahaly, G. Bonnaud, P. Martin, and F. Quéré, “Optical properties of relativistic plasma mirrors,” *Nature Communications*, vol. 5, no. 1, Mar. 2014, doi: https://doi.org/10.1038/ncomms4403.

[35] M. R. Bionta *et al.*, “Tracking ultrafast solid-state dynamics using high harmonic spectroscopy,” *Physical Review Research*, vol. 3, no. 2, Jun. 2021, doi: https://10.0.4.79/physrevresearch.3.023250.

[36] B. Wang, X. Li, and P. Fu, “Effect of a Static Electric Field on High-Harmonic Generation in a Polarized Laser Field,” *Chinese Physics Letters*, vol. 16, no. 10, pp. 723–725, Oct. 1999, doi: https://10.0.4.64/0256-307x/16/10/008.

[37] O. Finke *et al.*, “Phase-matched high-order harmonic generation in pre-ionized noble gases,” *Scientific Reports*, vol. 12, no. 1, May 2022, doi: https://doi.org/10.1038/s41598-022-11313-6.

[38] G. M. Rossi *et al.*, “Sub-cycle millijoule-level parametric waveform synthesizer for attosecond science,” *Nature Photonics*, vol. 14, no. 10, pp. 629–635, Jul. 2020, doi: https://doi.org/10.1038/s41566-020-0659-0.

[39] V. E. Nefedova, M. F. Ciappina, O. Finke, M. Albrecht, M. Kozlová, and J. Nejdl, “Efficiency control of high-order harmonic generation in gases using driving pulse spectral features,” *Applied Physics Letters*, vol. 113, no. 19, Nov. 2018, doi: https://doi.org/10.1063/1.5050691.

[40] J. Bauer, "High-order harmonic generation in model atoms: Comparison of one-dimensional and three-dimensional calculations," *Phys. Rev. A*, vol. 56, no. 4, pp. 3028–3036, Oct. 1997, doi: 10.1103/PhysRevA.56.3028.

[41] J. A. Pérez-Hernández, M. F. Ciappina, Maciej Lewenstein, L. Roso, and A. Zaïr, “Beyond CarbonK-Edge Harmonic Emission Using a Spatial and Temporal Synthesized Laser Field,” *Physical Review Letters*, vol. 110, no. 5, Jan. 2013, doi: https://doi.org/10.1103/physrevlett.110.053001.

[42] M. D. Feit, J. A. Fleck, and A. Steiger, “Solution of the Schrödinger equation by a spectral method,” *Journal of Computational Physics*, vol. 47, no. 3, pp. 412–433, Sep. 1982, doi: https://doi.org/10.1016/0021-9991(82)90091-2.

[43] J. L. Krause, K. J. Schafer, and K. C. Kulander, “Calculation of photoemission from atoms subject to intense laser fields,” *Physical Review A*, vol. 45, no. 7, pp. 4998–5010, Apr. 1992, doi: https://doi.org/10.1103/physreva.45.4998.

[44] A. M. Koushki, R Sadighi-Bonabi, M Mohsen-Nia, and E. Irani, “High-order harmonic generation of CO and N_2 molecules under linearly- and bi circularly-polarized laser pulses by TD-DFT,” *Laser physics*, vol. 28, no. 7, pp. 075404–075404, May 2018, doi: https://doi.org/10.1088/1555-6611/aabed5.